

Dirac semimetals $A_3\text{Bi}$ ($A = \text{Na, K, Rb}$) as \mathbb{Z}_2 Weyl semimetalsE. V. Gorbar,^{1,2} V. A. Miransky,³ I. A. Shovkovy,⁴ and P. O. Sukhachov¹¹*Department of Physics, Taras Shevchenko National Kiev University, Kiev 03680, Ukraine*²*Bogolyubov Institute for Theoretical Physics, Kiev 03680, Ukraine*³*Department of Applied Mathematics, Western University, London, Ontario, Canada N6A 5B7*⁴*College of Letters and Sciences, Arizona State University, Mesa, Arizona 85212, USA*

(Received 24 December 2014; revised manuscript received 12 February 2015; published 2 March 2015)

We demonstrate that the physical reason for the nontrivial topological properties of Dirac semimetals $A_3\text{Bi}$ ($A = \text{Na, K, Rb}$) is connected with a discrete symmetry of the low-energy effective Hamiltonian. By making use of this discrete symmetry, we argue that all electron states can be split into two separate sectors of the theory. Each sector describes a Weyl semimetal with a pair of Weyl nodes and broken time-reversal symmetry. The latter symmetry is not broken in the complete theory because the time-reversal transformation interchanges states from different sectors. Our findings are supported by explicit calculations of the Berry curvature. In each sector, the field lines of the curvature reveal a pair of monopoles of the Berry flux at the positions of Weyl nodes. The \mathbb{Z}_2 Weyl semimetal nature is also confirmed by the existence of pairs of surface Fermi arcs, which originate from different sectors of the theory.

DOI: [10.1103/PhysRevB.91.121101](https://doi.org/10.1103/PhysRevB.91.121101)

PACS number(s): 71.10.-w, 03.65.Vf, 71.15.Rf

Introduction. Three-dimensional (3D) Dirac semimetals whose conduction and valence bands touch only at discrete (Dirac) points in the Brillouin zone with the electron states described by the 3D massless Dirac equation are 3D analogs of graphene. Historically, bismuth [1] was the first material where it was shown that its low-energy quasiparticle excitations near the L point of the Brillouin zone are described by the 3D Dirac equation with a small mass [2]. Since the Dirac point is composed of two Weyl nodes of opposite chirality which overlap in momentum space, it can be gapped out. Therefore, even if the 3D Dirac point is obtained accidentally by fine tuning the spin-orbit coupling strength or chemical composition, it is, in general, not stable and is difficult to control.

It was proposed in Refs. [3,4] that an appropriate crystal symmetry can protect and stabilize the 3D Dirac points if two bands which cross each other belong to different irreducible representations of the discrete crystal rotational symmetry. By using the first-principles calculations and effective model analysis, $A_3\text{Bi}$ ($A = \text{Na, K, Rb}$) and Cd_3As_2 compounds were identified in Refs. [5,6] as 3D Dirac semimetals protected by crystal symmetry. Various topologically distinct phases can be realized in these compounds by breaking time-reversal and inversion symmetries. By making use of angle-resolved photoemission spectroscopy, a Dirac semimetal band structure was indeed observed [7–9] in Cd_3As_2 and Na_3Bi , opening the path toward the experimental investigation of the properties of 3D Dirac semimetals. For a recent review of 3D Dirac semimetals, see Ref. [10].

Closely related to 3D Dirac semimetals are Weyl semimetals. They were proposed to be realized in pyrochlore iridates [11], topological heterostructures [12], and magnetically doped topological insulators [13]. Although not experimentally observed yet, Weyl semimetals have been very actively studied theoretically (for reviews, see Refs. [14–16]). A Weyl node is topologically nontrivial because it is a monopole of the Berry flux in momentum space. This is also the reason why Weyl nodes can appear or annihilate only in pairs [17].

The simplest way to turn a Dirac semimetal into a Weyl one is to apply an external magnetic field, which breaks time-reversal symmetry. This can be realized even in the high-energy physics context [18]. In fact, the corresponding transition might have already been observed in $\text{Bi}_{1-x}\text{Sb}_x$ for $x \approx 0.03$ [19] and in Cd_3As_2 [20]. In the case of $\text{Bi}_{1-x}\text{Sb}_x$ [19], the authors measured negative magnetoresistivity at not very large magnetic fields that might be a fingerprint of a Weyl semimetal phase [17,21] (see, however, the discussion in Ref. [22]). In the case of Cd_3As_2 , a magnetic field driven splitting of Landau levels consistent with the Weyl phase, time-reversal symmetry breaking, and a nontrivial Berry phase were detected [20].

The existence of surface Fermi arcs [11,23–25] is another fingerprint of Weyl semimetals, associated with the nontrivial topology. Such arcs connect Weyl nodes of opposite chirality. The shape of the arcs depends on the boundary conditions and can be engineered [26]. The two Fermi arcs on opposite surfaces, together with the Fermi surface of bulk states, form a closed Fermi surface. This implies, in particular, that the chemical potentials for different chirality quasiparticles near distinct Weyl points must be the same in a static system [23].

Normally, one would not expect surface Fermi arcs in 3D Dirac semimetals because the Berry flux vanishes for Dirac points with vanishing topological charges. However, calculations of Refs. [5,6] suggest that Dirac semimetals $A_3\text{Bi}$ ($A = \text{Na, K, Rb}$) and Cd_3As_2 possess nontrivial surface Fermi arcs. This is an indication of a topologically nontrivial nature of these Dirac semimetals. In fact, as we argue below, the situation is reminiscent of topological insulators in which there is a \mathbb{Z}_2 topological order associated with the time-reversal symmetry [27–31]. This is further supported by the fact that the breaking of time-reversal or inversion symmetry in Dirac semimetals causes splitting of the surface Fermi arcs into a pair of open segments resembling the arcs in Weyl semimetals [5]. In this Rapid Communication, we explain the reason for the existence of nontrivial topological properties of the $A_3\text{Bi}$ compounds

and shed light on their analytical structure in the low-energy theory.

Hamiltonian. Our starting point in the analysis will be the low-energy effective Hamiltonian for electron excitations in $A_3\text{Bi}$ ($A = \text{Na, K, Rb}$) derived in Ref. [5]. The explicit form of the Hamiltonian is given by

$$H(\mathbf{k}) = \epsilon_0(\mathbf{k}) + H_{4 \times 4}, \quad (1)$$

$$H_{4 \times 4} = \begin{pmatrix} M(\mathbf{k}) & Ak_+ & 0 & B^*(\mathbf{k}) \\ Ak_- & -M(\mathbf{k}) & B^*(\mathbf{k}) & 0 \\ 0 & B(\mathbf{k}) & M(\mathbf{k}) & -Ak_- \\ B(\mathbf{k}) & 0 & -Ak_+ & -M(\mathbf{k}) \end{pmatrix}. \quad (2)$$

Note that the Hamiltonian of the same form is also valid for structure I of Cd_3As_2 (see Ref. [6]). The diagonal elements of the Hamiltonian are given in terms of two quadratic functions of momenta, $\epsilon_0(\mathbf{k}) = C_0 + C_1k_z^2 + C_2(k_x^2 + k_y^2)$ and $M(\mathbf{k}) = M_0 - M_1k_z^2 - M_2(k_x^2 + k_y^2)$. The off-diagonal elements are determined by the functions Ak_\pm and $B(\mathbf{k}) = \alpha k_z k_\pm^2$, where $k_\pm = k_x \pm ik_y$. The eigenvalues of Hamiltonian (1) are

$$E(\mathbf{k}) = \epsilon_0(\mathbf{k}) \pm \sqrt{M^2(\mathbf{k}) + A^2k_+k_- + |B(\mathbf{k})|^2}. \quad (3)$$

It is easy to check that the square root vanishes at the following two Dirac points, $\mathbf{k}_0^\pm = (0, 0, \pm \sqrt{m})$, where $m \equiv M_0/M_1$. The function $B(\mathbf{k})$, which can be interpreted as a momentum dependent mass term, also vanishes at the Dirac points.

The general considerations of the current study will apply to the compounds $A_3\text{Bi}$ ($A = \text{Na, K, Rb}$), but our numerical results will be presented for Na_3Bi . By fitting the energy spectrum of the effective Hamiltonian with the *ab initio* calculations for Na_3Bi , the following numerical values of the parameters in the effective model were extracted [5]: $C_0 = -0.06382 \text{ eV}$, $C_1 = 8.7536 \text{ eV \AA}^2$, $C_2 = -8.4008 \text{ eV \AA}^2$, $M_0 = -0.08686 \text{ eV}$, $M_1 = -10.6424 \text{ eV \AA}^2$, $M_2 = -10.3610 \text{ eV \AA}^2$, $A = 2.4598 \text{ eV \AA}$, and the lattice constants are $a = b = 5.448 \text{ \AA}$, $c = 9.655 \text{ \AA}$. Since no specific value for α was quoted in Ref. [5], we will treat it as a free parameter below. For most of our analysis below, however, the actual values of the model parameters are not very important. We will use them only when presenting some numerical results.

In the simplest case of a vanishing mass function $B(\mathbf{k})$ (or, equivalently, for $\alpha = 0$), the Hamiltonian $H_{4 \times 4}$ takes a block diagonal form, $H_{4 \times 4}(\alpha = 0) \equiv H_{2 \times 2}^+ \oplus H_{2 \times 2}^-$. Its upper block is given by

$$H_{2 \times 2}^+ = \begin{pmatrix} M(\mathbf{k}) & A(k_x + ik_y) \\ A(k_x - ik_y) & -M(\mathbf{k}) \end{pmatrix}, \quad (4)$$

and has a very transparent physical meaning. It defines the simplest version of a Weyl semimetal with two Weyl nodes located at \mathbf{k}_0^\pm . (The lower block $H_{2 \times 2}^-$ has a similar form, except that k_x is replaced by $-k_x$.) It is well known [25,32] that such a Weyl semimetal has the surface Fermi arc in the form of a straight line connecting Weyl nodes of opposite chirality at \mathbf{k}_0^+ and \mathbf{k}_0^- . Because of the sign difference, $k_x \rightarrow -k_x$, the chiralities of the states near the Weyl nodes at \mathbf{k}_0^\pm are opposite for the upper and lower block Hamiltonians. Thus, the complete 4×4 block diagonal Hamiltonian $H_{4 \times 4}(\alpha = 0)$

describes two superimposed copies of a Weyl semimetal with two pairs of overlapping nodes. The opposite chirality Weyl nodes coincide exactly in the momentum space and, thus, effectively give rise to two Dirac points at \mathbf{k}_0^\pm . At the same time, because the Weyl nodes come from different blocks, they cannot annihilate and cannot form topologically trivial Dirac points. In fact, the corresponding approximate model describes a \mathbb{Z}_2 Weyl semimetal. The nontrivial topological properties, associated with the underlying \mathbb{Z}_2 Weyl semimetal structure, ensure that the resulting Dirac semimetal possesses surface Fermi arcs.

It is easy to show that the existence of the \mathbb{Z}_2 Weyl semimetal structure in this simplest case is connected with the continuous symmetry $U_+(1) \times U_-(1)$ of the approximate Hamiltonian $H_{4 \times 4}(\alpha = 0)$. This symmetry describes independent phase transformations of the spinors that correspond to the block Hamiltonians $H_{2 \times 2}^+$ and $H_{2 \times 2}^-$, respectively.

Symmetries. It is well known that, for $B(\mathbf{k}) = \text{const}$, the symmetry $U_+(1) \times U_-(1)$ is broken to its diagonal subgroup $U_{\text{em}}(1)$ that describes the usual charge conservation. However, as we show below, the low-energy Hamiltonian (1) with the momentum dependent mass function $B(\mathbf{k}) = \alpha k_z k_\pm^2$ possesses a new discrete symmetry that protects the \mathbb{Z}_2 Weyl semimetal structure.

Before discussing this symmetry, let us start by pointing out that the Hamiltonian (1) is invariant under the time-reversal and inversion symmetries, i.e.,

$$\Theta H_{-\mathbf{k}} \Theta^{-1} = H_{\mathbf{k}} \quad (\text{time-reversal symmetry}), \quad (5)$$

$$P H_{-\mathbf{k}} P^{-1} = H_{\mathbf{k}} \quad (\text{inversion symmetry}), \quad (6)$$

where $\Theta = TK$ (K is a complex conjugation) and

$$T = \begin{pmatrix} 0 & 0 & 1 & 0 \\ 0 & 0 & 0 & 1 \\ -1 & 0 & 0 & 0 \\ 0 & -1 & 0 & 0 \end{pmatrix}, \quad P = \begin{pmatrix} 1 & 0 & 0 & 0 \\ 0 & -1 & 0 & 0 \\ 0 & 0 & 1 & 0 \\ 0 & 0 & 0 & -1 \end{pmatrix}. \quad (7)$$

Of course, these two symmetries are expected in Dirac semimetals such as $A_3\text{Bi}$, and they do play an important role in understanding their physical properties. The less obvious is the following symmetry defined by the transformation,

$$U H_{-k_z} U^{-1} = H_{k_z} \quad (\text{ud parity}), \quad (8)$$

where matrix U has the following block diagonal form, $U \equiv \text{diag}(I_2, -I_2)$ and I_2 is the 2×2 unit matrix. We call it the up-down (ud) parity because its eigenstates for $B(\mathbf{k}) = 0$ in view of the block-diagonal structure of Hamiltonian (2) correspond to bispinors with only two upper or lower nonzero components that describe a Weyl semimetal with a pair of Weyl nodes. It should be noted that, for the Hamiltonian to be invariant under this symmetry, it is crucial that the mass function $B(\mathbf{k})$ changes its sign when $k_z \rightarrow -k_z$ [while the functions $\epsilon_0(\mathbf{k})$ and $M(\mathbf{k})$ in the diagonal elements do not change their signs]. Were the mass function momentum independent, such a discrete symmetry would not exist.

The existence of the time-reversal (5) and ud parity (8) symmetries has an important implication that we will now explain. The argument relies on the fact that all quasiparticle

states in the low-energy model of a Dirac semimetal naturally split into two separate groups, classified by the eigenvalues of the operator $U_\chi = U\Pi_{k_z}$. (Here, Π_{k_z} is the operator that changes the sign of the z component of momentum, $k_z \rightarrow -k_z$.) Taking into account that $U_\chi^2 = 1$, the eigenvalues of U_χ are ± 1 . Furthermore, the corresponding eigenstates are *not* invariant under time reversal. This follows from the fact that the operators of time-reversal Θ and U_χ parity transformations do not commute. This implies that each sector of quasiparticle states with a fixed eigenvalue of U_χ defines a distinct copy of the Weyl semimetal, for which time reversal is broken. Of course, the time-reversal symmetry is not broken in the complete system including both U_χ sectors. In view of the U_χ symmetry, we can classify the corresponding Dirac semimetal as a \mathbb{Z}_2 Weyl semimetal. The situation resembles that of topological insulators [27–31], which are time-reversal invariant due to the \mathbb{Z}_2 topological order parameter.

Each Weyl subsystem, described by quasiparticle states with a fixed eigenvalue of U_χ , has well defined Fermi arcs connecting the Weyl nodes at \mathbf{k}_0^\pm . These arcs are topologically protected and cannot be removed by small perturbations of model parameters.

In our discussion of Fermi arcs, it will be also useful to take into account that there exists yet another discrete symmetry defined by the following transformation,

$$\tilde{U}H_{-k_x}\tilde{U}^{-1} = H_{k_x}, \quad (9)$$

where

$$\tilde{U} = \begin{pmatrix} 0 & 0 & 1 & 0 \\ 0 & 0 & 0 & 1 \\ 1 & 0 & 0 & 0 \\ 0 & 1 & 0 & 0 \end{pmatrix}. \quad (10)$$

Of course, the product of the U_χ and $\tilde{U}\Pi_{k_x}$ transformations $U_\chi\tilde{U}\Pi_{k_x} = T\Pi_{k_x}\Pi_{k_z}$ is also a symmetry of the low-energy Hamiltonian (1). Note that the symmetry $T\Pi_{k_x}\Pi_{k_z}$ is related to the time-reversal symmetry if we take into account that $K\Pi_{k_y}$ is also the symmetry of Hamiltonian (1). Together, the operators U_χ , $\tilde{U}\Pi_{k_x}$, and $T\Pi_{k_x}\Pi_{k_z}$ form a noncommutative discrete group.

Eigenstates of U_χ . Since Hamiltonian (1) commutes with U_χ , its eigenstates with eigenvalues $E(\mathbf{k})$ given by Eq. (3) can be chosen as eigenstates of U_χ , too (alternatively, we can choose the energy eigenstates to be eigenstates of the $\tilde{U}\Pi_{k_x}$ or $T\Pi_{k_x}\Pi_{k_z}$ symmetries). These eigenstates have the following form:

$$\psi_+(\mathbf{k}) = N_+ \begin{pmatrix} 1 \\ \frac{E(\mathbf{k}) - \epsilon_0(\mathbf{k}) - M(\mathbf{k})}{A k_+} \\ \frac{B(\mathbf{k})}{A k_+} \\ 0 \end{pmatrix}, \quad (11)$$

$$\psi_-(\mathbf{k}) = N_- \begin{pmatrix} -\frac{B^*(\mathbf{k})}{A k_-} \\ 0 \\ 1 \\ -\frac{E(\mathbf{k}) - \epsilon_0(\mathbf{k}) - M(\mathbf{k})}{A k_-} \end{pmatrix}. \quad (12)$$

Here N_\pm are normalization constants and the subscript \pm means the eigenvalue of U_χ . It is not difficult to check that $\tilde{U}\Pi_{k_x}$ transforms ψ_+ into ψ_- and vice versa. Notice that

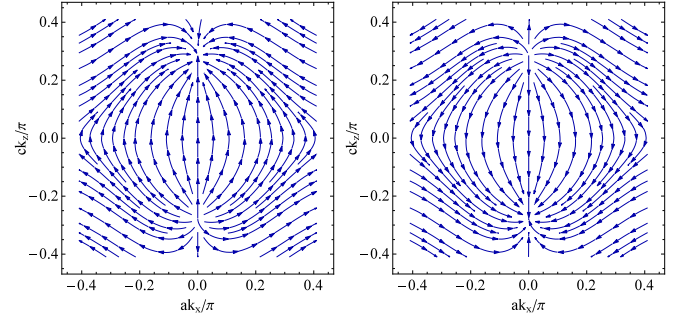


FIG. 1. (Color online) The projection of the Berry curvature $\mathbf{F}_{++}(\mathbf{k})$ (left panel) and $\mathbf{F}_{--}(\mathbf{k})$ (right panel) on the $k_y = 0$ plane.

the bispinors ψ_\pm in the case with a vanishing mass function, $B(\mathbf{k}) = 0$, describe fermions of definite chirality in the vicinity of the \mathbf{k}_0^\pm points.

Berry curvature. In order to explicitly reveal the \mathbb{Z}_2 Weyl semimetal structure of $A_3\text{Bi}$ ($A = \text{Na, K, Rb}$), we calculated the Berry connection and the Berry curvature for each sector described by the $\psi_\pm(\mathbf{k})$ states. Due to the double degeneracy of the states with the same energy in the present case, the Berry curvature is a matrix with non-Abelian gauge structure [33],

$$\begin{aligned} \mathbf{A}_{mn}(\mathbf{k}) &\equiv -\frac{i}{2}[\psi_m^\dagger(\mathbf{k})(\nabla_{\mathbf{k}}\psi_n(\mathbf{k})) - (\nabla_{\mathbf{k}}\psi_m^\dagger(\mathbf{k}))\psi_n(\mathbf{k})], \\ \mathbf{F}_{mn}(\mathbf{k}) &\equiv \nabla_{\mathbf{k}} \times \mathbf{A}_{mn} - i\mathbf{A}_{ml} \times \mathbf{A}_{ln}, \end{aligned} \quad (13)$$

where $m, n, l = \pm$ and the summation over l is performed in the last equation. The four components of the Berry connection $\mathbf{A}_{mn}(\mathbf{k})$ define a $U(2)$ gauge field. The Berry curvature components $\mathbf{F}_{++}(\mathbf{k})$ and $\mathbf{F}_{--}(\mathbf{k})$ are plotted in Fig. 1. The numerical results are shown for $\alpha = 50 \text{ eV \AA}^3$ and the energy eigenvalue in Eq. (3) with the positive sign in front of the square root. (Up to the change of direction of the vector fields, the plots for the other sign of root look qualitatively the same.)

The results for the diagonal components of the curvature in Fig. 1 show that each sector with a definite eigenvalue of U_χ contains a pair of Berry curvature monopoles with charges ± 1 . Such a dipole structure in the momentum space is an unambiguous signature of a Weyl semimetal in each of the sectors.

We would like to emphasize that the presence of the mass function $B(\mathbf{k})$ does not affect the property of the diagonal Berry curvature $\mathbf{F}_{++}(\mathbf{k})$ [or $\mathbf{F}_{--}(\mathbf{k})$] to have nonzero divergencies at the Weyl nodes. Mathematically, the qualitative behavior of the curvature in the vicinity of the nodes is preserved because $B(\mathbf{k})$ vanishes at \mathbf{k}_0^\pm . Away from the Weyl nodes, on the other hand, the mass function does affect the behavior of the Berry curvature. This is already seen in Fig. 1, where slight distortions of the dipole configurations become visible. It can be checked that distortions become much stronger at larger values of parameter α . We found, however, that the opposite charge monopoles of the Berry flux remain well resolved even for α as large as 250 eV \AA^3 .

It is interesting to point out that the off-diagonal components of the Berry curvature $\mathbf{F}_{+-}(\mathbf{k})$ [as well as $\mathbf{F}_{-+}(\mathbf{k})$] are nonzero only because of the nontrivial mass function $B(\mathbf{k})$. The

complete implications of this fact remain to be investigated. This task, however, is beyond the scope of the present Rapid Communication.

Surface Fermi arcs. The nontrivial topological structure of the ψ_+ and ψ_- sectors implies that the $A_3\text{Bi}$ compounds should have surface Fermi arcs. Previously, the surface Fermi arcs in these 3D Dirac semimetals were studied in Ref. [5] by using an iterative method to obtain the surface Green's function of the semi-infinite system [34]. The imaginary part of the surface Green's function makes it possible to determine the local density of states at the surface. In our study here, we employ the continuum low-energy model and enforce appropriate boundary conditions for the quasiparticle spinors at the surface of the semimetal. As we will argue, such a consideration makes the physical properties of the surface Fermi arc states more transparent.

We assume that semimetal is situated at $y \geq 0$ and is infinite in the x and z directions. The simplest implementation of the boundary condition for the semimetal states on its surface follows from the replacement of m with $-\tilde{m}$ and taking the limit $\tilde{m} \rightarrow \infty$ on the vacuum side of the boundary [25]. Taking into account that the Fermi arc states should be localized at the $y = 0$ boundary, we can look for the surface state solution in the following form,

$$\Psi(\mathbf{r}) = \Psi_1 e^{-p_1 y} + \Psi_2 e^{-p_2 y}, \quad (14)$$

where Ψ_i can be chosen as the eigenstates of the U_x symmetry and p_i are the positive (that are necessary for the normalization of the wave function) roots of the characteristic equation

$$\begin{aligned} & [C_2(k_x^2 - p^2) + C_1 k_z^2 + C_0 - E]^2 + A^2(p^2 - k_x^2) \\ & - [M_0 - M_1 k_z^2 - M_2(k_x^2 - p^2)]^2 - \alpha^2 k_z^2 (p^2 - k_x^2)^2 = 0. \end{aligned} \quad (15)$$

The wave function on the vacuum side has a similar form, but with the replacement $p_i \rightarrow -\tilde{p}_i$, where the definition of \tilde{p}_i is similar to that of p_i , but m is replaced by $-\tilde{m}$. (In the calculation, we take the limit $\tilde{m} \rightarrow \infty$, which prevents quasiparticles from escaping into vacuum.)

Matching the wave functions across the boundary, we obtain the following equation,

$$(Q_1^+ - Q_2^+)(Q_1^- - Q_2^-) - (T_1^+ - T_2^+)(T_1^- - T_2^-) = 0, \quad (16)$$

where

$$Q_i^\pm = -\frac{C_2(k_x^2 - p_i^2) + C_1 k_z^2 + C_0 - E \mp A k_x}{M_0 - M_1 k_z^2 - M_2(k_x^2 - p_i^2) - A p_i}, \quad (17)$$

$$T_i^\pm = -\frac{\alpha k_z (p_i \pm k_x)^2}{M_0 - M_1 k_z^2 - M_2(k_x^2 - p_i^2) - A p_i}. \quad (18)$$

The numerical solutions for the surface Fermi arcs are shown in Fig. 2 for several fixed values of the Fermi energy and $\alpha = 1 \text{ eV \AA}^3$. In the special case of $E = 0$, our results are in qualitative agreement with the results obtained in Ref. [5] by using a different method.

Other materials. By combining the first-principles calculations and effective model analysis, it was recently predicted [35] that the ternary compounds BaYBi ($Y = \text{Au, Ag, Cu}$) are

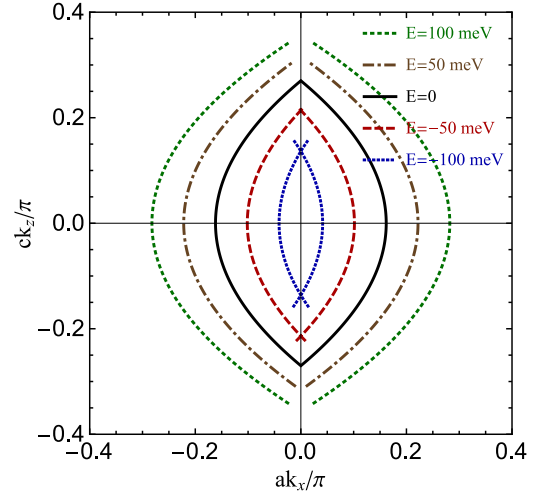


FIG. 2. (Color online) The surface Fermi arcs for $\alpha = 1 \text{ eV \AA}^3$ and energy $E = 0, \pm 50, \pm 100 \text{ meV}$.

Dirac semimetals. The low-energy effective Hamiltonian of these compounds is similar to that of $A_3\text{Bi}$ ($A = \text{Na, K, Rb}$), but with a different structure of the mass terms,

$$H_{\text{ternary}} = \epsilon_0(\mathbf{k}) + H'_{4 \times 4}, \quad (19)$$

where

$$H'_{4 \times 4} = \begin{pmatrix} M(\mathbf{k}) & Ak_+ & 0 & Bk_z k_+^2 \\ Ak_- & -M(\mathbf{k}) & -Bk_z k_+^2 & 0 \\ 0 & -Bk_z k_-^2 & M(\mathbf{k}) & Ak_- \\ Bk_z k_-^2 & 0 & Ak_+ & -M(\mathbf{k}) \end{pmatrix}. \quad (20)$$

Since Hamiltonian (19) is invariant with respect to the U_x symmetry transformation, our conclusions remain valid for these compounds. Thus, these Dirac semimetals are \mathbb{Z}_2 Weyl semimetals, too.

In conclusion, as we argued in this Rapid Communication, Dirac semimetals $A_3\text{Bi}$ ($A = \text{Na, K, Rb}$) are, in fact, \mathbb{Z}_2 Weyl semimetals. The conclusion is supported by the existence of the ud parity U_x that allows us to split all states into two sectors, with each describing a Weyl semimetal. It is the combination of both sectors that gives rise to a \mathbb{Z}_2 Weyl character of the corresponding semimetals. Naturally, the time-reversal and inversion symmetries are preserved in such a theory. The situation might be reminiscent of topological insulators, where the topological order is protected by the time-reversal symmetry [27–31].

The symmetry arguments used in the current study are rather powerful. They suggest that the main conclusions should remain unchanged even in the presence of interaction effects, provided the latter do not modify the low-energy spectrum in a qualitative way. A weak disorder [36] and a subcritical Coulomb interaction [37] are examples of such effects that exist in realistic materials, but are not expected to change our main conclusions.

The fact that the compounds $A_3\text{Bi}$ ($A = \text{Na, K, Rb}$) are \mathbb{Z}_2 Weyl semimetals has important implications. On the one hand, it sheds light on the existence of surface Fermi arcs in such materials. This is particularly important in view of the recent experimental confirmation of such states in Na_3Bi [38].

Additionally, it predicts the same types of quantum oscillations as in true Weyl semimetals [32], with the period dependent on the thickness of the semimetal slabs. Indeed, when the two Weyl sectors are protected from mixing by the \mathbb{Z}_2 symmetry, their contributions will simply superimpose. Furthermore, when the time reversal is broken (e.g., by magnetic impurities), we anticipate that the superposition of two oscillations with nonequal periods will be observed.

The work of E.V.G. was supported partially by the Ukrainian State Foundation for Fundamental Research. The work of V.A.M. was supported by the Natural Sciences and Engineering Research Council of Canada. The work of I.A.S. was supported by the U.S. National Science Foundation under Grant No. PHY-1404232 and in part by the Chinese Academy of Sciences Visiting Professorship for Senior International Scientists.

-
- [1] M. H. Cohen and E. I. Blount, *Philos. Mag.* **5**, 115 (1960).
 [2] P. A. Wolff, *J. Chem. Phys. Solids* **25**, 1057 (1964).
 [3] S. M. Young, S. Zaheer, J. C. Y. Teo, C. L. Kane, E. J. Mele, and A. M. Rappe, *Phys. Rev. Lett.* **108**, 140405 (2012).
 [4] J. L. Manes, *Phys. Rev. B* **85**, 155118 (2012).
 [5] Z. Wang, Y. Sun, X. Q. Chen, C. Franchini, G. Xu, H. Weng, X. Dai, and Z. Fang, *Phys. Rev. B* **85**, 195320 (2012).
 [6] Z. Wang, H. Weng, Q. Wu, X. Dai, and Z. Fang, *Phys. Rev. B* **88**, 125427 (2013).
 [7] S. Borisenko, Q. Gibson, D. Evtushinsky, V. Zabolotnyy, B. Buchner, and R. J. Cava, *Phys. Rev. Lett.* **113**, 027603 (2014).
 [8] M. Neupane, S.-Y. Xu, R. Sankar, N. Alidoust, G. Bian, C. Liu, I. Belopolski, T.-R. Chang, H.-T. Jeng, H. Lin, A. Bansil, F. Chou, and M. Z. Hasan, *Nat. Commun.* **5**, 3786 (2014).
 [9] Z. K. Liu, B. Zhou, Y. Zhang, Z. J. Wang, H. M. Weng, D. Prabhakaran, S.-K. Mo, Z. X. Shen, Z. Fang, X. Dai, Z. Hussain, and Y. L. Chen, *Science* **343**, 864 (2014).
 [10] Q. D. Gibson, L. M. Schoop, L. Muechler, L. S. Xie, M. Hirschberger, N. P. Ong, R. Car, and R. J. Cava, [arXiv:1411.0005](https://arxiv.org/abs/1411.0005).
 [11] X. Wan, A. M. Turner, A. Vishwanath, and S. Y. Savrasov, *Phys. Rev. B* **83**, 205101 (2011).
 [12] A. A. Burkov and L. Balents, *Phys. Rev. Lett.* **107**, 127205 (2011).
 [13] G. Y. Cho, [arXiv:1110.1939](https://arxiv.org/abs/1110.1939).
 [14] A. A. Burkov, M. D. Hook, and L. Balents, *Phys. Rev. B* **84**, 235126 (2011).
 [15] A. M. Turner and A. Vishwanath, [arXiv:1301.0330](https://arxiv.org/abs/1301.0330).
 [16] O. Vafek and A. Vishwanath, *Annu. Rev. Condens. Matter Phys.* **5**, 83 (2014).
 [17] H. B. Nielsen and M. Ninomiya, *Phys. Lett. B* **130**, 389 (1983).
 [18] E. V. Gorbar, V. A. Miransky, and I. A. Shovkovo, *Phys. Rev. C* **80**, 032801 (2009).
 [19] H.-J. Kim, K.-S. Kim, J. F. Wang, M. Sasaki, N. Satoh, A. Ohnishi, M. Kitaura, M. Yang, and L. Li, *Phys. Rev. Lett.* **111**, 246603 (2013).
 [20] J. Cao, S. Liang, C. Zhang, Y. Liu, J. Huang, Z. Jin, Z.-G. Chen, Z. Wang, Q. Wang, J. Zhao, S. Li, X. Dai, J. Zou, Z. Xia, L. Li, and F. Xiu, [arXiv:1412.0824](https://arxiv.org/abs/1412.0824).
 [21] D. T. Son and B. Z. Spivak, *Phys. Rev. B* **88**, 104412 (2013).
 [22] E. V. Gorbar, V. A. Miransky, and I. A. Shovkovo, *Phys. Rev. B* **89**, 085126 (2014).
 [23] F. D. M. Haldane, [arXiv:1401.0529](https://arxiv.org/abs/1401.0529).
 [24] V. Aji, *Phys. Rev. B* **85**, 241101 (2012).
 [25] R. Okugawa and S. Murakami, *Phys. Rev. B* **89**, 235315 (2014).
 [26] P. Hosur, *Phys. Rev. B* **86**, 195102 (2012).
 [27] M. Konig, S. Wiedmann, C. Brune, A. Roth, H. Buhmann, L. W. Molenkamp, X.-L. Qi, and S.-C. Zhang, *Science* **318**, 766 (2007).
 [28] D. Hsieh, D. Qian, L. Wray, Y. Xia, Y. S. Hor, R. J. Cava, and M. Z. Hasan, *Nature (London)* **452**, 970 (2008).
 [29] C. L. Kane and E. J. Mele, *Phys. Rev. Lett.* **95**, 146802 (2005).
 [30] M. Z. Hasan and C. L. Kane, *Rev. Mod. Phys.* **82**, 3045 (2010).
 [31] X.-L. Qi and S.-C. Zhang, *Rev. Mod. Phys.* **83**, 1057 (2011).
 [32] A. C. Potter, I. Kimchi, and A. Vishwanath, *Nat. Commun.* **5**, 5161 (2014).
 [33] F. Wilczek and A. Zee, *Phys. Rev. Lett.* **52**, 2111 (1984).
 [34] W. Zhang, R. Yu, H. J. Zhang, X. Dai, and Z. Fang, *New J. Phys.* **12**, 065013 (2010).
 [35] Y. Yu, B. Wan, D. Wang, L. Sheng, C.-G. Duan, and X. Wan, [arXiv:1411.4394](https://arxiv.org/abs/1411.4394).
 [36] B. Roy and S. Das Sarma, *Phys. Rev. B* **90**, 241112(R) (2014).
 [37] J. Gonzalez, *Phys. Rev. B* **90**, 121107(R) (2014).
 [38] S.-Y. Xu, C. Liu, S. K. Kushwaha, R. Sankar, J. W. Krizan, I. Belopolski, M. Neupane, G. Bian, N. Alidoust, T.-R. Chang, H.-T. Jeng, C.-Y. Huang, W.-F. Tsai, H. Lin, P. P. Shibayev, F.-C. Chou, R. J. Cava, and M. Z. Hasan, *Science* **347**, 294 (2015).